EVALUATION OF INTERFACIAL PROPERTIES AND DAMAGE SENSING ON CFRP BY VARTM USING 3-DIMENSIONAL ELECTRICAL RESISTANCE MAPPING

J. H. Kim[1], D. J. Kwon[1], P. S. Shin[1], K. L. DeVries[2],
J. M. Park[1, 2*]
[1] School of Materials Science and Engineering, Engineering Research Institute,
Gyeongsang National University, Jinju, Korea
[2] Department of Mechanical Engineering, The University of Utah, Salt Lake City, U. S. A.
* Corresponding author (jmpark@gnu.ac.kr)

Keywords: *VARTM, Permeability, Interfacial property, 3D ER mapping*

ABSTRACT

In the research reported here CFRC plates were manufactured using two different resins, epoxy and unsaturated polyester (UP), by a vacuum assisted resin transfer molding (VARTM) process. The permeability, as indicated by the spreading difference via VARTM, was measured for two composites with the same fiber volume fraction but different viscosities. The interfacial properties of the CFRC, manufactured using these different resins, were evaluated utilizing the interlinear shear strength (ILSS) test and contact angle measurements. Three dimensional electrical resistance (3D ER) mapping was used to detect damage caused by the drilling of holes in the CFRC plates.

1 INTRODUCTION

This is due primarily to poor fiber/resin interfacial adhesion attributed to the poor wetting and adsorption ability of carbon fiber with most resins because the carbon fiber surface is non-polar and composed of highly crystallized graphitic basic planes. The interfacial bonding strength between the carbon fibers and the resin matrix is rather low making it difficult to obtain good mechanical properties in composites [1, 2].

The manufacture of composite parts to be joined and assembled with other parts in automotive structures often requires drilling of holes in the composite parts. However, the delamination and thermal damage typically associated with drilling processes raises the risk of component damage and failure during the service lifecycle [3]. The unique properties of CFRP like the stiff and abrasive carbon fiber and the heat sensitive matrix make the machining process more challenging. Due to the abrasiveness of the carbon fiber, tool wear immediately sets in resulting in a rapid decrease in hole quality. Damage at and near the hole, such as delamination, fiber pull-out, matrix melting or micro cracks either on the exit or entry side as well as on the hole wall may, be caused by the degrading tool [4, 5].

One type of self-sensing technology applies an electric current (EC) to composite structures and measures changes in electrical resistance (ER) to detect damage [6]. ER measurement hve been used to evaluate micro-damage leading to changes in mechanical properties via in situ ER or EC measurements while stresses are applied to the composite [7]. Although this self-sensing technique can effectively detect damage, it requires the mounting of many electrodes on the CFRC surface [8]. There is, therefore, a demand for a new method that detects delamination cracking over a wide area with a smaller number of electrodes. Recently, in research by Park et. al. [9], in situ 2D ER mapping was developed and used for sensing damage, its location, the distribution of CF contact and breakage in CF reinforced thermoplastic composites.

In this study, CFRC plates were manufactured, using two types of resins (epoxy and UP), using the VARTM process. The permeability by VARTM was measured for the two composites with the same fiber volume fraction but different viscosities. The interfacial properties of CFRC using the different resins were evaluated by an ILSS test. This new method of 3D (by expanding from 2D) ER mapping

was evaluated as a means of detecting damage caused during hole fabrication in CFRC.

2 EXPERIMENTAL

2.1 Materials

Unidirectional carbon fiber (CF) mat (PX35, Zoltek Corporation, U.S.A.) was used as the composite reinforcement. Bisphenol-A type epoxy (KER-9100, Kumho P&B Chemicals Inc., Korea), amine type curing agent (KCA-9110, Kumho P&B Chemicals Inc., Korea) and poly (vinyl ester) (DION-9100A, Aekyung Chemical Co. Ltd., Korea) were used as matrices for the composites. Six layers of carbon fiber mat were piled in the 0°, 90° directions and copper wires were arranged at each corner in 1st and 5th layers. The CFRC was manufactured by the VARTM process with a fiber volume fraction of 50%.

2.2 Methodologies

2.2.1 Permeability, viscosity, and contact angle measurements of CFRC

Permeability was measured as the degree of spreading of CF laminate specimens to compare the interfacial properties for the two different resins [10, 11]. As indicated by equation (1) parameters affecting permeability are also viscosity, surface tension and contact angle as well as processing conditions such as injection pressure, flow rate and temperature [12].

$$K_f = -q_f \cdot \mu \cdot h_f / P_f \tag{1}$$

Where, K_f is permeability of the CF mat, q_f is the flow distance of resin into the CF mat, μ is viscosity of the resin, h_f is the thickness of the laminated CF mat and P_f is the pressure on the CF mat. The fiber volume fraction was kept constant at V_f = 50% for all permeability measurements. In each experiment a specimen composed of a stack of reinforcement layers which were in the form of a pile up of 0°, 90° oriented CF was used.

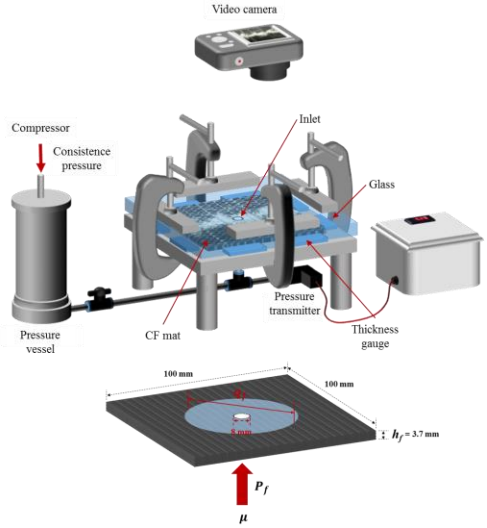

Figure 1: Schematic of permeability measurement

A schematic plot of the arrangement used for permeability measurements is shown in Figure 1. The viscosity was measured using a viscometer (DV-2+pro, Brookfield Engineering Inc., U.S.A.) with a rotating spindle. A resin inlet hole with 8 mm diameter was located in the center of the specimen. After the CF mats were laid upon the permeability measurement table, the CF mat was tighten using 4 clamps to produce a uniform thickness of CF mat as measured using a gauge. Resin was injected into CF mat via the inlet hole and a pressure vessel was used to maintain a constant resin flow rate into the CF mat. The pressure on the fibers was measured using a pressure transmitter (PA-21Y, Keller AG fuer Druckmesstechnik, Switzerland) while the resin flow rate and flow distance into the CF mat were observed, using a video camera.

Static contact angles were measured to observe the initial and the change of static contact angle

with elapsing time, thereby providing a comparison of spreading of the resins in the CF mat. Resin drops of approximately 1 mm size was dropped onto the CF mat using a syringe and the static contact angles of resin drops were was measured in situ, using a reflecting microscope (AM4113ZT, Anmo Electronics Corporation, Taiwan).

2.2.2 Damage sensing of CFRC using 3D ER mapping

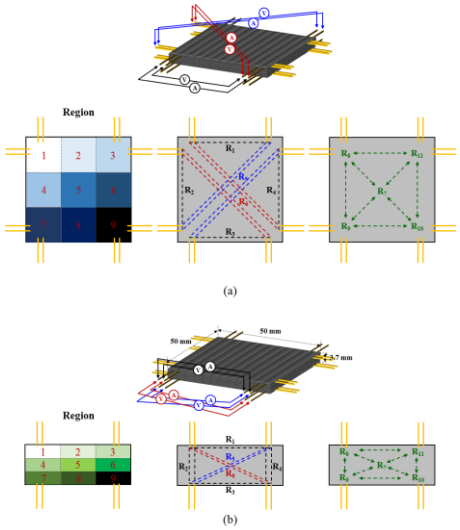

Figure 2: Arrangement of 3D ER mapping on a 1 cell ER: (a) X, Y axis; (b) Z axis

Figure 2 shows a schematic plot of a 9 part arrangement in a single cell used for ER 3D mapping. Six layers of CF mat were piled with an alternating 0°, 90° orientation and a copper wire arranged at the edges of the 1st and 5th layers. The size of mapping specimen was 50 mm length, 50 mm width, and 3.7 mm thickness. Specimens were prepared with two types of resin (epoxy and UP) by injection into carbon fiber mats using a vacuum pump (YTP20G, Ulvac Tech. Inc., U.S.A.). The cell, used for the ER measurement, was a square area containing 32 probe connectors arranged so that at each corner of the 1st and 5th layers there was a connection to a multimeter (Agilent Co. Ltd., U.S.A.). Hole fabrication was performed using a hand drill (IXO, Robert Bosch Tool Co., Germany) with a 2 mm diameter drill bit. The 2 mm diameter holes were drilled to the following three depths: 1.2 mm, 2.4 mm and 3.7 mm, in both the CF/epoxy and CF/UP specimens. Throughout this drilling operation the variation in ER was measured using the multimeter.

Figure 2(a) displays 2D ER mapping schemes for X-Y axis square area specimens. The ERs along the X-Y axis of these areas were measured using 16 probes in each specimen. Figure 2(b) illustrated the 2D ER mapping scheme for the X-Z axis of a specimen. ERs of the X-Z axis of a specimen's area were measured using a total of 8 probes in a specimen. The surface of the specimen were divided into 9 ER regions that were evaluated using 2D ER mapping to develop contour or surface charts. The sketches and equations (2) to (6) illustrate the various ERs which were measured, evaluated and analyzed/determined with the aid of a commercial Excel program and used in the ER mapping. Segments from R_1 to R_4, designated by black lines, R_5 designated by blue lines and R_6 designated by red lines in Figure 2 (b) were measured directly for use in the data reduction with the excel program. R_5 and R_6 were for the diagonal segments while R_8, R_9, R_{10}, R_{11} were calculated to represent the ER for the segments outlined by the green lines, which was recently published by Park's group [18]. By combining 2D ER mapping of X-Y axis area and 2D ER mapping of X-Z axis area, 3D ER mapping could be obtained.

$$R_7 = (R_5 + R_6) / 2 \quad (2)$$

$$R_8 = (R_1 + R_2 + R_7) / 3 \quad (3)$$

$$R_9 = (R_2 + R_3 + R_7) / 3 \quad (4)$$

$$R_{10} = (R_3 + R_4 + R_7) / 3 \quad (5)$$

$$R_{11} = (R_4 + R_1 + R_7) / 3 \quad (6)$$

2.2.3 Mechanical property and ILSS measurements using specimen of Mapping

Tensile test of epoxy and UP were performed to measure Young's modulus of resin with 3 times. Tensile and 3 point bending tests were performed with 0.3 mm/minute and based on ASTM D-638 standards. ILSS was measures and evaluated based on the short beam test (ASTM D-2344) by using cut above ER mapping specimen. The specimen's dimensions were: 30 mm length, 10 mm width, and 3.7 mm thickness. Specimens for the short beam test were manufactured by VARTM and equation (7) was used to calculate the ILSS [13].

$$ILSS = 3F / 4bd \quad (7)$$

Where F is the applied force, while b and d are the thickness and width of the test specimen. The experimental set up for the ILSS test is as a bending test with a span of 20 mm and a test speed of 3 mm/minute. The results given are an average of at three tests.

3. RESULTS AND DISCUSSION

3.1 PERMEABILITY, VISCOSITY AND CONTACT ANGLE FOR TWO RESINS ON CF MAT

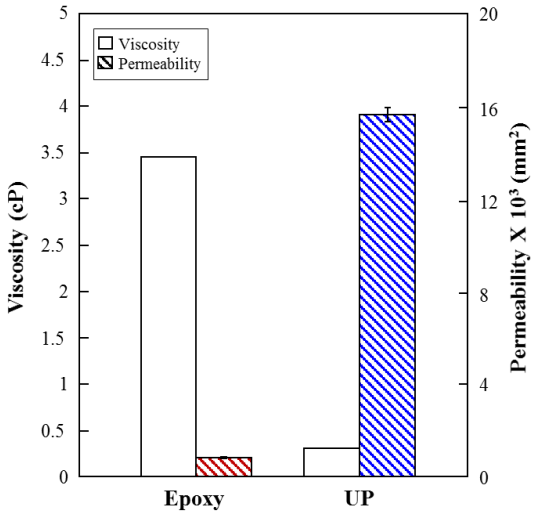

Figure 3: Viscosity and permeability of epoxy and UP

Figure 3 shows the viscosity and permeability for epoxy and UP in CF mat. The viscosity of the epoxy was 3.45 cP which was more than ten times compared to the viscosity of 0.3 cP for UP. On the other hand, the permeability of epoxy in CF was approximately 1 x 10^3 mm^2 whereas it was roughly 15 x 10^3 mm^2 for UP in CF. The permeability of the epoxy was less than a tenth than that of the UP. Epoxy in CF exhibited a much higher viscosity and much lower permeability than UP in CF. It can be said that viscosity and permeability are intimately correlated, although other parameters, such as surface tension, contact angle, injection pressure, flow rate and temperature affect the permeability as well.

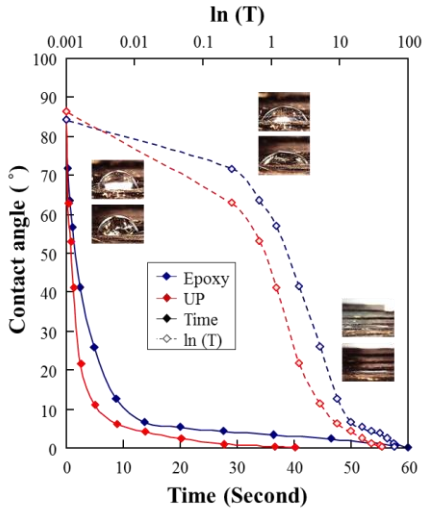

Figure 4: Static contact angle change for resin and CF mat in-situ

Figure 4 shows the static contact angle change of the resin for CF mat with elapsing time. Contact angles are widely used for investigating chemical and physical surface characteristics of materials [14]. The initial static contact angle of a UP droplet was 86° whereas static contact angle of epoxy droplet was 84°. Initially the contact angles of the two resins are very similar, suggesting that the interfacial affinity of epoxy close to that of UP. However, with elapsing time, the static contact angle of UP decreases significantly more rapidly than it does for epoxy. This suggests that the UP penetrates more rapidly into the CF mat than the epoxy does which can likely be attributed to epoxy's higher viscosity.

3.2 DAMAGE SENSING OF DRILLED CFRC VIA 3D ER MAPPING

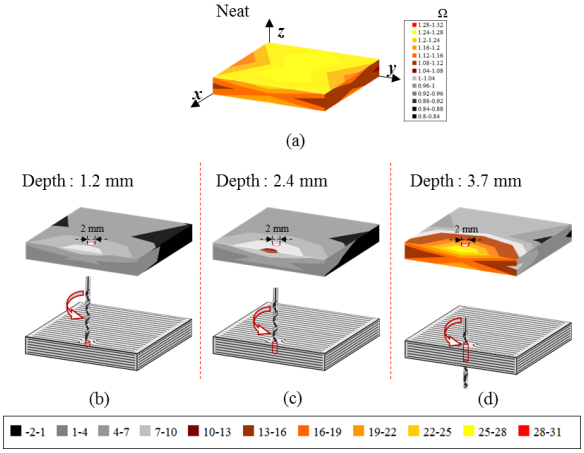

Figure 5: 3D ER mapping as depth of hole: (a) Neat CF/epoxy composite; (b) 1.2 mm; (c) 2.4 mm; and (d) 3.7 mm

Figure 5 shows the 3D ER mapping results with increasing depth of the drilled hole in a CF/epoxy composite surface. Figure 5(a) shows the neat ER mapping results before drilling and Figure 5(b) to (d) exhibits 3D ER mapping during steps in drilling depth. For the initial drilling to depth of 1.2 mm, the color of X-Y and X-Z axis surfaces exhibited a rather bright gray appearance with a slightly different gray appearance around the hole. With further drilling from 1.2 mm to 2.4 mm depth, the colors of X-Y and X-Z axis surfaces changed from bright to dark brown accompanied by expansion of the light gray area. For the X-Z axis area, the gray color was expanded as a result of hole fabrication. Figure 5(d) shows mapping for further drilling to 3.7 mm depth (completely through the specimen thickness). After the penetration, the color of X-Y and X-Z axis area was changed to yellowish and bright gray color appearances at the X-Z surface. The authors feel that these results are an indication

of the potential utility of 3D ER mapping.

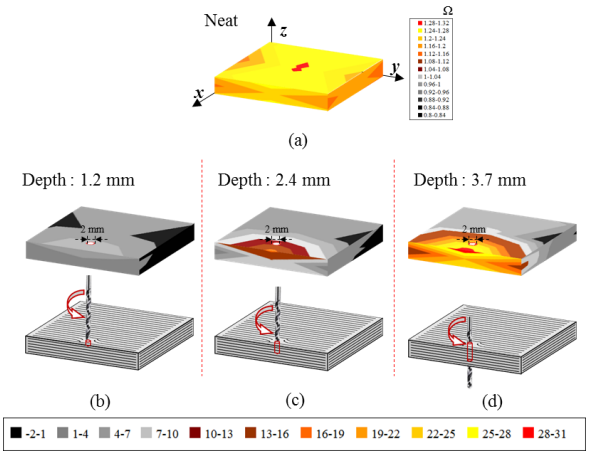

Figure 6: 3D ER mapping as a function of depth of hole: (a) Neat CF/UP composite; (b) 1.2 mm; (c) 2.4 mm; and (d) 3.7 mm

Figure 6 shows 3D ER mapping results with increasing depth of drilled holes in CF/UP composites. Comparing CF/epoxy in Figure 5 with CF/UP composites in Figure 6, the color changes in 3D ER mapping for CF/epoxy composites were less than for the CF/UP composites. The 3D ER mapping results for CF/UP composite were broader with more color change than for CF/epoxy composite. The more ER color change and broader ER range implies more damage in the specimen. This indicates that during drilling the CF/epoxy composite experienced less damaged than the CF/UP composite. This might be attributed, in part, to the higher inherent modulus of the epoxy.

3.3 VISUAL OBSERVATION OF THE HOLES AFTER DRILLING-COMMENTS ON CFRC

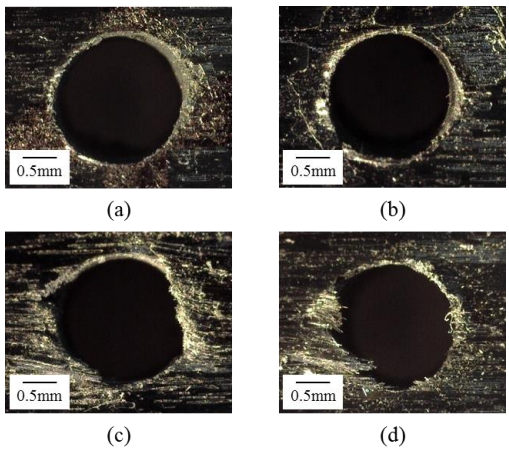

Figure 7: Observation after drilling of hole: (a) upper part of hole in CF/epoxy; (b) lower part of hole in CF/epoxy; (c) upper part of hole in CF/UP; and (d) lower part of hole in CF/UP

Figure 7 shows optically the nature of the holes after drilling of CFRC. Figure 7 (a) and 7(b) show views of the top and bottom of a hole in a specimen of a CF/epoxy composite specimen while 7(c) and 7(d) show similar views of the top and bottom of a hole in a CF/UP composite specimen. The shape of the hole of the CF/epoxy composite specimen was relatively clean while drilling in the CF/UP composite specimen produced a much rougher hole and indications of delamination in the lower left of both photos for CF/UP. The effects demonstrated in these Figure are attributed to CF/epoxy composites having a greater ILSS than CF/UP composites.

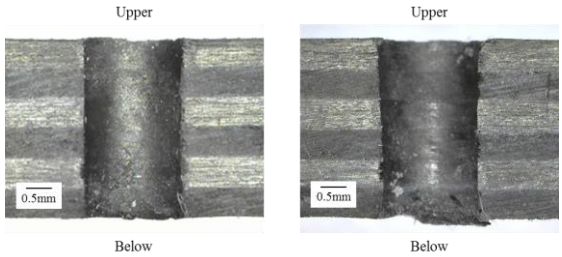

Figure 8: Observation of Cross section observation of hole: (a) CF/epoxy; (b) CF/UP

Figure 8 shows the cross section of the two composites after drilling holes. Again it is seen that in the CF/epoxy composite the drilling produced a rather uniform smooth hole except for some small fluff. Consistent with the photos in and associated discussion of Figure 7 drilling of CF/UP, produced a hole with a somewhat irregular diameter and with significant signs of delamination particularly near the lower part of the hole.

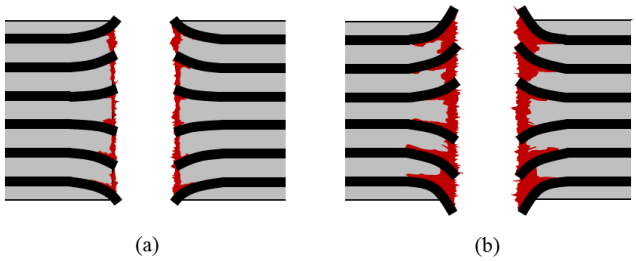

Figure 9: Schematic of CF deformation in CFRP to drilling of a hole: CF/epoxy composite; (b) CF/UP composite

Figure 9 shows schematic models of carbon fiber deformation in CFRC after drilling a hole. Drilling induces shear stresses in the composites near the periphery of the drill. These stresses might cause delamination, the extent of which would be dependent on the ILSS. One would anticipate that such damage would cause localized increases in the ER measurements and 3D ER mapping, discussed previously.

3.4 MECHANICAL PROPERTIES AND ILSS TEST

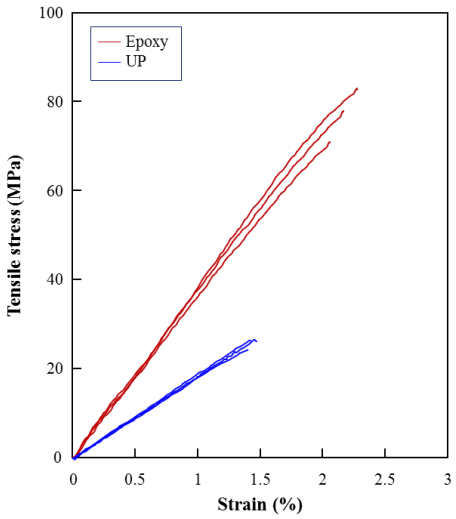

Figure 10: Results of tensile tests of epoxy and UP

Figure 10 shows the mechanical properties of the epoxy and UP. Tensile strength of the epoxy was 71.7 MPa and strain was 2.16 % whereas tensile strength of the UP was only 24.4 MPa and strain was

1.49 %. Since tensile modulus of epoxy was 36 GPa whereas tensile modulus of the UP was only 16.4 GPa, the UP exhibited higher ductility than epoxy.

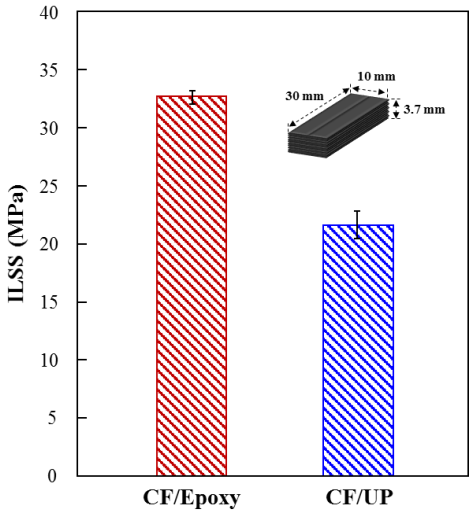

Figure 11: Results of ILSS tests on CF/epoxy and CF/UP composites

Figure 11 shows the ILSS for the CF/epoxy and CF/UP composites. The ILSS of the CF/epoxy composites was 33 MPa whereas the ILSS of the CF/UP composites was only 22 MPa. During the drilling process, it was also observed that the ER measurements for the CF/epoxy composites was more uniform with less scatter than it was for the CF/epoxy composites which exhibited a larger error range bar. This correlation reveals that the CF/epoxy composite had not only better ILSS but was also structurally more stable than the CF/UP composite.

4 CONCLUSIONS

Interfacial damage induced by drilling in two different epoxy and UP composites was detected and evaluated via 3D ER mapping during the drilling operation. Damage, particularly interfacial failure was related to the ILSS of CF/epoxy and CF/UP composites. Permeability, viscosity and static contact angle measurements were also correlated for the drilling processing and damage produced in epoxy and UP based composites. While epoxy had poorer permeability than UP, the CF/epoxy composite exhibited better ILSS than the CF/UP composite. While initial contact angle measurement indicated that the interfacial affinity of epoxy and UP with the mat surface were with time the static contact angle of UP decreased more rapidly steeply than for did epoxy. It was observed that UP penetrates more easily and rapidly into CF mat than does epoxy. This is attributed to the higher viscosity of the epoxy. The interfacial properties and permeability were not directly proportional to each but the permeability could be rather strongly affected by viscosity. 3D ER mapping was used to detect and evaluate damage during hole fabrication in the CF/epoxy and CF/UP composites. 3D ER mapping results, in conjunction with optical inspection, revealed that this damage involved extensive delamination at the interface between CFs. The CF/epoxy composite exhibited better interfacial properties than the CF/UP composite and the UP exhibited higher ductility than epoxy. When the CFRC structure was damaged the damaged area and depth, was relatively easily and successfully detected via a 3D ER mapping method. This method might be usefully applicable to other damage causes and modes in CFRCs.

ACKNOWLEDGMENTS

This work (No.C0397829) was supported by Business for Cooperative R&D between Industry, Academy, and Research Institute funded Korea Small and Medium Business Administration in 2016-2017. This work was also supported by the BK21 Plus Program (Future-oriented innovative brain raising type, 21A20151713274) funded by the Ministry of Education (MOE, Korea) and National Research Foundation (NRF), Korea.

REFERENCES

[1] Zhang X, Pei X, Wang Q, The tribological properties of acid- and diamine-modified carbon fiber reinforced polyimide composites. Mater Chem Phys 2009;115:825-830

[2] Kingsley KCH, Beamson G, Shia G, Polyakova NV., Bismarck A, Surface and bulk properties of severely fluorinated carbon fibres. J Fluor Chem 2007;128: 1359-1368

[3] Liu DF, Tang YJ, Cong WL, A review of mechanical drilling for composite laminates. Compos Struct 2012;94:1265-1279

[4] Gaugel S, Sripathy P, Haeger A, Meinhard D, Bernthaler T, Lissek F, Kaufeld M, Knoblauch V, Schneoder G, A comparative study on tool wear and laminate damage in drilling of carbon-fiber reinforced polymers (CFRP). Compos Struct 2016;155:173-183

[5] Li NY, Li YG, Zhou J, He YX, Hao XZ, Drilling delamination and thermal damage of carbon nanotube/carbon fiber reinforced epoxy composites processed by microwave curing. Int J Mach Tool Manu 2015;97:11-17

[6] Xia Z, Okabe T, Park JB, Curtin WA, Takeda N, Quantitative damage detection in CFRP composites: coupled mechanical and electrical models. Compos Sci Techno 2003;63:1411-1422

[7] Todoroki A, Yamada K, Mizutani Y, Suzuki Y, Matsuzaki R, Impact damage detection of a carbon-fibre-reinforced-polymer plate employing self-sensing time-domain reflectometry. Compos Struct 2015;130:174-179

[8] Milad H, Mohammad PG, A new sensing skin for qualitative damage detection in concrete elements: Rapid difference imaging with electrical resistance to mography. NDT E Int 2014;68:13-21

[9] Kwon DJ, Shin PS, Kim JH, DeVries KL, Park JM, Evaluation of dispersion and damage sensing of carbon fiber/polypropylene (PP)-polyamide (PA) composites using 2 dimensional electrical resistance mapping. Compos Part A 2016;90:417-423

[10] Um MK, Lee SK, Kim TW, Kim JH, Koh SW, A study on the determination of in-plane permeability of fiber preforms. Compos Res 1998;11:75-83

[11] Naik NK, Sirisha M, Inani A, Permeability characterization of polymer matrix composites by RTM/VARTM. Prog Aerosp Sci 2014;65:22-40

[12] Ameri E, Lebrun G, Laperriere L, In-plane permeability characterization of a unidirectional flax/paper reinforcement for liquid composite molding processes. Compos Part A 2016;85:52-64

[13] ASTM. Standard test method for short-beam strength of polymer matrix composite materials and their laminates, Designation D 2344/D 2344M; 2006

[14] Park JM, Kwon DJ, Wang ZJ, Kim JJ, Jang KW, DeVries KL, New method for interfacial evaluation of carbon fiber/thermosetting composites by wetting and electrical resistance measurements. J Adhes Sci Technol 2014;28:1677-1686